Spinel $LiNi_{0.5}Mn_{1.5}O_4$ Cathode for High-Energy Aqueous Lithium-Ion Batteries

*Fei Wang, Liumin Suo, Yujia Liang, Chongyin Yang, Fudong Han, Tao Gao, Wei Sun, and Chunsheng Wang**

Lithium ion batteries (LIBs) have been widely acknowledged as the high-energy battery system for grid storage and electric vehicles, but the safety concern due to the flammability of organic electrolytes still hinders their wide application.[1–3] To address the issue, aqueous lithium-ion batteries (ALIBs) using nonflammable and low-toxic aqueous electrolytes are receiving intense attention as the alternatives.[4–8] The aqueous electrolytes also make it possible to get rid of the rigorous moisture-free manufacturing environment and heavy reliance on the battery management systems at module or pack levels. Since the voltage of ALIBs is intrinsically limited by the narrow thermodynamic stability window of aqueous electrolyte, the ALIBs have a much lower energy density (40 W h kg^{-1}) than that of LIBs (200 W h kg^{-1}).[9,10]

Despite of over two decades' materials innovation, the battery community has not witnessed much progress in improving the capacity of ALIBs' electrodes. The most effective method in increasing the energy density is to enhance cell voltage by enlarging the electrochemical stability window of aqueous electrolytes and identifying viable electrode materials. Recently, our group has made a significant breakthrough in doubling electrochemical stability window of aqueous electrolyte from 1.5 to 3.0 V (1.9–4.9 V)[11] using water-in-salt electrolytes. A 2.3 V $LiMn_2O_4/Mo_6S_8$ full cell using water-in-salt electrolytes was demonstrated to cycle up to 1000 times, with nearly 100% coulombic efficiency at both a low (0.15 C) and a high (4.5 C) discharge and charge rates.[11] However, $LiMn_2O_4$ with lithiation/delithiation potential of 4.2 V does not fully use the oxygen evolution potential of 4.9 V in water-in-salt electrolytes. Commercial spinel $LiNi_{0.5}Mn_{1.5}O_4$ with $P4_332$ structure has a higher operating voltage (a slope plateau from 4.6 to 4.8 V for a continuous redox reaction of $Ni^{2+/3+/4+}$ in organic electrolyte) than $LiMn_2O_4$ (single plateau of 4.2 V).[12,13] $LiNi_{0.5}Mn_{1.5}O_4$ should provide much high energy in water-in-salt electrolyte since it has similar capacity with $LiMn_2O_4$. However, due to the high salt concentration of the water-in-salt electrolytes, the redox lithiation/delithiation potential plateau of $LiNi_{0.5}Mn_{1.5}O_4$ positively shifts by ≈0.2V[11] to 4.8–5.0 V, which is over the edge of the stable window of electrolyte. The single plateau of $P4_332$ $LiNi_{0.5}Mn_{1.5}O_4$ can only provide <50% of capacity if considering the overpotential during charge process. Recently, Yamada et al. reported that $LiNi_{0.5}Mn_{1.5}O_4$ can only reversibly provide capacity of ≈75 mA h g^{-1} in the more concentrated hydrate melt electrolytes (≈30 mol kg^{-1}), which is 50% of theoretical capacity.[14] The oxygen evolution side reaction also largely significantly reduce the coulombic efficiency.

In addition to $P4_332$ structure, $LiNi_{0.5}Mn_{1.5}O_4$ also has another structure with the space groups of Fd-3m. In $P4_332$ $LiNi_{0.5}Mn_{1.5}O_4$, all Mn-ions exist as Mn^{4+}, while in Fd-3m $LiNi_{0.5}Mn_{1.5}O_4$, small amount of Mn^{3+} coexists along with Mn^{4+}.[15] The larger ionic radius of Mn^{3+} compared to Mn^{4+} expands lattice, enhancing the Li+ diffusion.[16] The structure difference in $LiNi_{0.5}Mn_{1.5}O_4$ also changes the lithiation/delithiation potentials.[17] Fd-3m $LiNi_{0.5}Mn_{1.5}O_4$ has two distinguished plateaus at 4.6 V ($Ni^{2+/3+}$) and 4.8 V($Ni^{3+/4+}$). The 4.6 V of redox $Ni^{2+/3+}$ can be fully utilized since it is completely inside the electrolyte stable window even taking consideration of the potential shift. Although the 4.8 V plateau shifts to 5.0 V, which is beyond the 4.9 V window of water-in-salt electrolyte, part capacity of $LiNi_{0.5}Mn_{1.5}O_4$ at 5.0 V can still be achieved due to the fast lithiation reaction in Fd-3m $LiNi_{0.5}Mn_{1.5}O_4$ and slow oxygen evolution reaction. If the pH value of electrolyte can be reduced, all the capacity can potentially be utilized.

In the present work, the electrochemical behaviors of two $LiNi_{0.5}Mn_{1.5}O_4$ cathodes with Fd-3m and $P4_332$ structures in the water-in-salt electrolytes were systematically investigated. After screening, $LiNi_{0.5}Mn_{1.5}O_4$ with Fd-3m structure was selected and paired with Mo_6S_8 anode. A 2.9 V $LiNi_{0.5}Mn_{1.5}O_4/Mo_6S_8$ ALIB delivered 80 W h kg^{-1} energy density with capacity decay only 0.075% per cycle (5 C). After reducing the pH value of the water-in-salt electrolyte from 7 to 5, almost full capacity of $LiNi_{0.5}Mn_{1.5}O_4$ (125 mA h kg^{-1}) was achieved in the aqueous electrolyte for the first time, and 126 W h kg^{-1} energy density was provided for the $LiNi_{0.5}Mn_{1.5}O_4/Mo_6S_8$ full cell, representing one of the highest voltage and energy density among all the aqueous batteries reported so far.

$LiNi_{0.5}Mn_{1.5}O_4$ with Fd-3m or $P4_332$ structures were synthesized according to the previous literatures.[13,18,19] X-ray diffraction (XRD) Rietveld refinements confirm the two different structures (**Figure 1**a,b). By carefully comparing the XRD in Figure 1a,b, two small super lattice peaks at 15.3° and 39.7° are observed in $P4_332$ $LiNi_{0.5}Mn_{1.5}O_4$ in Figure 1b but they are absent in Fd-3m $LiNi_{0.5}Mn_{1.5}O_4$ in Figure 1a. The structure difference between two $LiNi_{0.5}Mn_{1.5}O_4$ was further enhanced by transferring the XRD patterns of the two structures into Log 10 intensity (Figure S1, Supporting Information). The structure difference between Fd-3m and $P4_332$ $LiNi_{0.5}Mn_{1.5}O_4$ is also captured by Raman spectrum, where more peaks are observed in the $P4_332$ $LiNi_{0.5}Mn_{1.5}O_4$ (Figure 1e) than that in

Dr. F. Wang, Dr. L. Suo, Y. Liang, Dr. C. Yang, F. Han, T. Gao, W. Sun, Prof. C. Wang
Department of Chemical and Biomolecular Engineering
University of Maryland
College Park, MD 20742, USA
E-mail: cswang@umd.edu

DOI: 10.1002/aenm.201600922

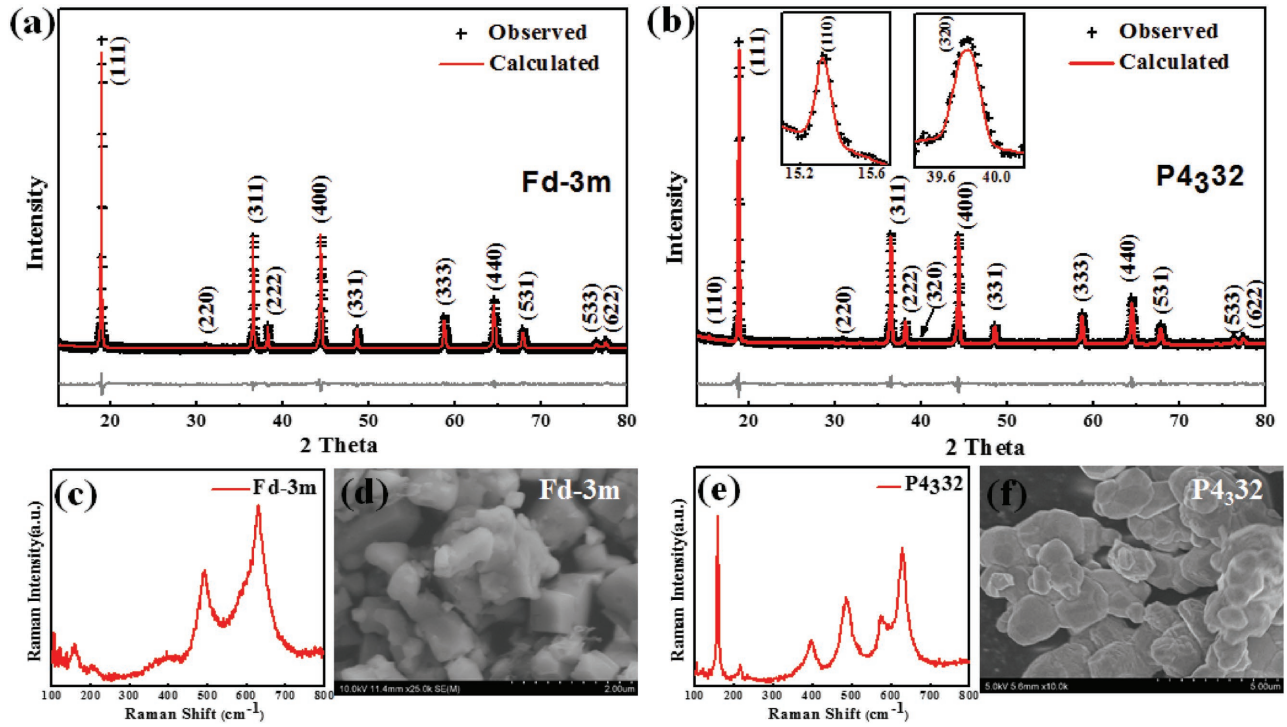

Figure 1. Rietveld refinement profiles of XRD data for a) $LiNi_{0.5}Mn_{1.5}O_4$ powder with Fd-3m group and b) $P4_332$ group. c) Raman spectra and d) SEM image for $LiNi_{0.5}Mn_{1.5}O_4$ powder with Fd-3m group. e) Raman spectra and f) SEM image for $LiNi_{0.5}Mn_{1.5}O_4$ powder with $P4_332$ group.

the Fd-3m $LiNi_{0.5}Mn_{1.5}O_4$ (Figure 1c). Two $LiNi_{0.5}Mn_{1.5}O_4$ materials also have different morphology as demonstrated by scanning electron microscopy (SEM) images in Figure 1d,f. Flat planes with well-defined edges are observed in the SEM image for the Fd-3m particles in Figure 1d, while the $P4_332$ $LiNi_{0.5}Mn_{1.5}O_4$ (Figure 1f) is less defined smooth particles. All XRD, Raman, and SEM analysis confirm that we successfully synthesized two pure $LiNi_{0.5}Mn_{1.5}O_4$ with Fd-3m and $P4_332$ space groups.

The electrochemical stability window of water-in-salt electrolytes was measured by cyclic voltammetry (CV) using stainless steel grid as both working and counter electrodes, and the Ag/AgCl as a reference electrode. As shown in **Figure 2**a, a stability window of ≈3.0 V is achieved, with cathodic limit at ≈1.9 V (vs Li) and anodic limit at ≈4.9 V (vs Li). In addition to largely enlarging electrochemical stability window of the aqueous electrolytes,[20–24] increasing the salt concentration in the aqueous solutions can also increase the lithiation/delithiation potential of the electrodes. The lithiation/delithiation potentials of Fd-3m $LiNi_{0.5}Mn_{1.5}O_4$ and $P4_332$ $LiNi_{0.5}Mn_{1.5}O_4$ were also evaluated by CV in the same water-in-salt electrolyte using active carbon as a counter electrode and the Ag/AgCl as a reference electrode. As shown

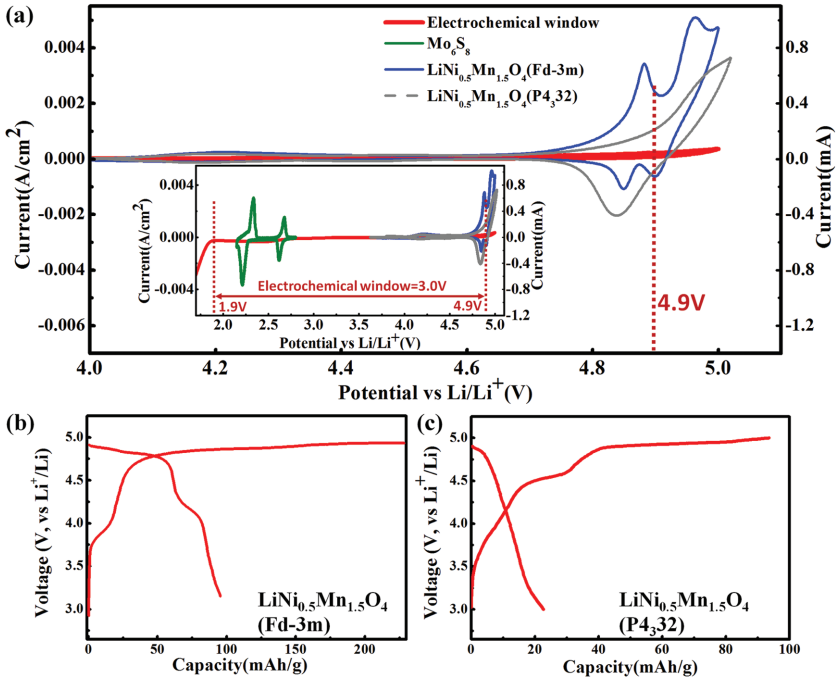

Figure 2. a)The electrochemical window of water-in-salt electrolytes as measured on stainless steel current collector at scanning rate of 10 mV s^{-1} and the lithiation/delithiation potentials of Mo_6S_8 anode and the $LiNi_{0.5}Mn_{1.5}O_4$ cathode with different crystal structures measured were measured at scanning rate of 0.1 mV s^{-1} in the same electrolyte. b,c) The typical voltage profile of $LiNi_{0.5}Mn_{1.5}O_4$ in water-in-salt at constant current of 0.5 C with $LiTi_2(PO_4)_3$ as anode and the Ag/AgCl as the reference electrode.

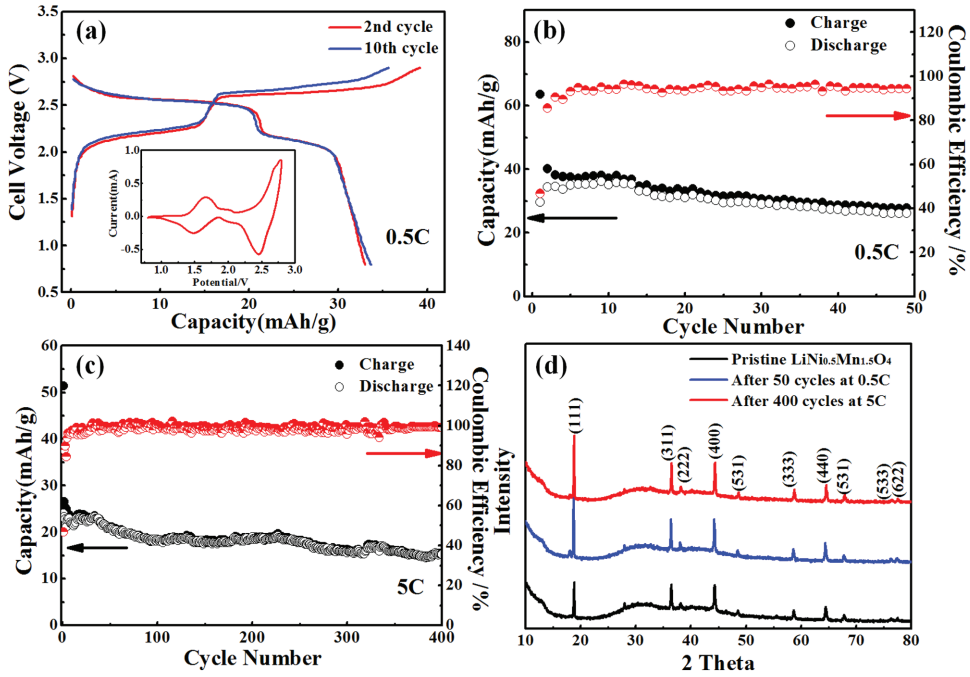

Figure 3. a) The typical voltage profile of the full aqueous Li-ion cell employing Mo_6S_8 and $LiNi_{0.5}Mn_{1.5}O_4$ as anode and cathode in water-in-salt electrolytes at a constant current of 0.5 C (inset the CV curves for the full cell). b,c) The cycling stability and Coulombic efficiencies of full cells at low (0.5 C) and high (5 C) rates. d) The XRD patterns for the $LiNi_{0.5}Mn_{1.5}O_4$ electrodes before and after cycling.

in the CV results (Figure 2a), the Fd-3m $LiNi_{0.5}Mn_{1.5}O_4$ exhibits two well-resolved redox peaks at 4.88/4.85 V and 4.96/4.90 V, while only one redox peak at 5.02/4.85 V is observed in the $P4_332$ $LiNi_{0.5}Mn_{1.5}O_4$ electrodes. The first redox peaks potential (4.88/4.85 V) of Fd-3m $LiNi_{0.5}Mn_{1.5}O_4$ is less than the anodic stability potential (4.9 V). However, the redox peak of $P4_332$ space (5.02 V) is out of the electrolyte window (4.9 V), thus the Li extraction process will accompany with very strong electrolyte decomposition when more than half of the lithium is delithiated. The galvanostatic lithiation/delithiation behaviors of $LiNi_{0.5}Mn_{1.5}O_4$ were also evaluated in water-in-salt electrolytes using a three-electrode cell with excess $LiTi_2(PO_4)_3$ as a counter electrode (capacity of $LiTi_2(PO_4)_3$ is much higher than that of $LiNi_{0.5}Mn_{1.5}O_4$) and Ag/AgCl as a reference electrode. The use of $LiTi_2(PO_4)_3$ as the counter electrode is because the lithiation/delithiation plateaus of $LiTi_2(PO_4)_3$ is very flat and well-inside of the stability window of water-in-salt electrolytes (Figure S2, Supporting Information). Figure 2b,c shows the galvanostatic lithiation/delithiation behaviors of Fd-3m $LiNi_{0.5}Mn_{1.5}O_4$ and $P4_332$ $LiNi_{0.5}Mn_{1.5}O_4$ in water-in-salt electrolytes at 0.5 C of current density. After fully charged to 4.9 V (vs Li^+/Li), the discharge of Fd-3m $LiNi_{0.5}Mn_{1.5}O_4$ shows a long potential plateau at about 4.8 V followed by a small slope at 4.2 V providing total discharge capacity of 98 mA h g^{-1} (Figure 2b). In contrast, the $P4_332$ $LiNi_{0.5}Mn_{1.5}O_4$ shows a small discharge capacity of 20 mA h g^{-1} since the most of its potential plateau is out of the electrolyte window (Figure 2c). Therefore, $LiNi_{0.5}Mn_{1.5}O_4$ with Fd-3m structure was selected as the high-voltage cathode to fabricate the high-voltage aqueous full cell.

Our previous work showed that the Chevrel phase Mo_6S_8 (Figures S3 and S4, Supporting Information) can stably cycle in water-in-salt electrolytes over 1000 times.[11] Thus, Mo_6S_8 was used as an anode to pair with Fd-3m $LiNi_{0.5}Mn_{1.5}O_4$ cathode. The $LiNi_{0.5}Mn_{1.5}O_4/Mo_6S_8$ mass ratio was set to 5:2 in order to compensate the irreversible capacity loss due to the formation of solid electrolyte interphase (SEI) on the Mo_6S_8 anode during the initial cycles (Figure S5, Supporting Information).[11] As shown in **Figure 3**a, the open circuit of fully charged $LiNi_{0.5}Mn_{1.5}O_4/Mo_6S_8$ full cell is 2.9 V. The discharge of $LiNi_{0.5}Mn_{1.5}O_4/Mo_6S_8$ cell at 0.5 C displays two voltage plateaus at 2.6 and 2.2 V since Mo_6S_8 anode has two reversible redox couples of Li^+ lithiation/delithiation at 2.43/2.24 V and 2.75/2.67 V, as shown in the CV in Figure 2a. The $LiNi_{0.5}Mn_{1.5}O_4/Mo_6S_8$ cell delivers a discharge capacity of 34 mA h g (of total electrode mass) and an energy density of 80 W h kg^{-1}. A maximum of 140 W h Kg^{-1} can be reached by optimizing the electrodes ratio and reduction of the initial irreversible capacity.

The cycling stability of $LiNi_{0.5}Mn_{1.5}O_4/Mo_6S_8$ cell was evaluated at both low and high currents. In most studies, the cycling stability of ALIBs was normally evaluated at a high cycling current to minimize the damage of hydrogen/oxygen evolution to cycling stability.[25,26] In fact, the most rigorous proof of stability does not come from the number of cycles, but from the time spent by a system at a fully charged state as well as from high coulombic efficiency at low C rates.[5,27] Figure 3b,c displays the cycling stability and coulombic efficiency of $LiNi_{0.5}Mn_{1.5}O_4/Mo_6S_8$ full cells at both low (0.5 C) and high (5 C) rates. Excellent cycling stability with a capacity decay rate of 0.2% per cycle at 0.5 C and 0.07% per cycle at 5 C is observed. Due to the formation of the SEI on the Mo_6S_8 anode surface,[11] the coulombic efficiency in the first cycle is low, but it quickly increases to 96% after 10 cycles at the 0.5 C rate. The coulombic efficiency increases to near 100% when SEI is completely coated on Mo_6S_8 surface at the 5 C for 50 cycles.

The open-circuit-voltage decay of fully charged cells during storage was also monitored and the ratio of discharged capacity to charged capacity after 24 h storage was measured to evaluate the self-discharge and H_2/O_2 evolution rates. The high capacity tetain ratio of 93.3% in Figure S6 (Supporting Information) confirmed the negligible hydrogen or oxygen evolution and high coulombic efficiency of $LiNi_{0.5}Mn_{1.5}O_4/Mo_6S_8$ full cell. The structure evolution of $LiNi_{0.5}Mn_{1.5}O_4$ during the charge/discharge cycles in the aqueous electrolyte was also investigated using ex situ XRD (Figure 3d). Both the $LiNi_{0.5}Mn_{1.5}O_4$ cycled either after 50 times at a low rate of 0.5 C or after 400 times a high rate of 5 C have the same structure as the pristine $LiNi_{0.5}Mn_{1.5}O_4$ electrode.

Although the Fd-3m $LiNi_{0.5}Mn_{1.5}O_4$ in 21m water-in-salt electrolytes delivered a higher capacity (98 mA h g^{-1}) than that (75 mA h g^{-1}) of $P4_332$ $LiNi_{0.5}Mn_{1.5}O_4$ in the hydrate melt electrolytes (≈30 m),[14] the full capacity of $LiNi_{0.5}Mn_{1.5}O_4$ is still not achieved. The oxygen evolution potential of the water-in-salt electrolyte need to be positively shifted further. It is well known that both the hydrogen and oxygen evolution potentials in aqueous electrolyte will shift to higher voltage along with the decrease of the pH value.[5,10] Since the low (second) potential (2.1 V) of Mo_6S_8 is still higher than the hydrogen evolution potential (1.9 V) of the water-in-salt electrolyte, we reduced the pH value of the water-in-salt electrolyte to 5 by adding 0.1% (in volume) 1 M bis(trifluoromethane sulfonyl) imide ($HN(SO_2CF_3)_2$, HTFSI), which positively shifted the window by 0.1 V. As shown in **Figure 4**a,b, the Fd-3m $LiNi_{0.5}Mn_{1.5}O_4$ in pH 5 water-in-salt electrolyte can stably deliver a high discharge capacity of 125 mA h g^{-1} after charged to 5.05 V (vs Li^+/Li), which is more close to its theoretical capacity (147 mA h g^{-1}). Coupled with Mo_6S_8, the full cell could achieve a high energy density of 126 W h kg^{-1} (Figure 4b).

The energy density and the cycle life of the $LiNi_{0.5}Mn_{1.5}O_4/Mo_6S_8$ full cell were compared to all reported ALIBs in Figure 4c,[5,9,28–32] in which the cycling stability is color-coded with red, blue, and green representing <100 cycles, 100–500 cycles, and >1000 cycles, respectively. Although $LiMn_2O_4$/active carbon[31] and $LiFePO_4/LiTi_2(PO_4)_3$[10] cells can charge/discharge for 1000 cycles their energy density (<50 W h kg^{-1}) is too low. On the other hand, some high-energy cells with voltage to ≈1.50 V suffer from poor cycling stability.[9] The open circuit of the $LiNi_{0.5}Mn_{1.5}O_4/Mo_6S_8$ full cell can achieve 3.0 V with energy density of 126 W h kg^{-1} (based on two electrodes) which is one of the highest among all the ALIBs reported to date.

The aqueous $LiNi_{0.5}Mn_{1.5}O_4/Mo_6S_8$ Li-ion battery is also compared to other types of aqueous batteries and nonaqueous Li-ion batteries. Figure 4 d shows the voltage and energy density of the aqueous electrolyte rechargeable batteries and some non-aqueous Li-ion batteries (based on the electrode material). The nickel-metal hydride (Ni-MH) and Zn-MnO_2 batteries using concentrated KOH electrolyte deliver 1.2 and 1.5 V, respectively. By taking advantage of the electrodes with high H_2 and O_2 overpotential, lead-acid batteries can achieve 2 V of voltage.[33] Up to today, among all the commercial aqueous systems, only lead-acid battery can achieve 2.0 V but its energy density is less than 50 W h kg^{-1}. The $LiNi_{0.5}Mn_{1.5}O_4/Mo_6S_8$ full cell represents one of the highest voltage and highest energy density among all aqueous rechargeable batteries (Figure 4c,d), which is even comparable with nonaqueous $LiFePO_4$-$Li_4Ti_5O_{12}$ and $LiMn_2O_4$-$Li_4Ti_5O_{12}$ Li-ion batteries.

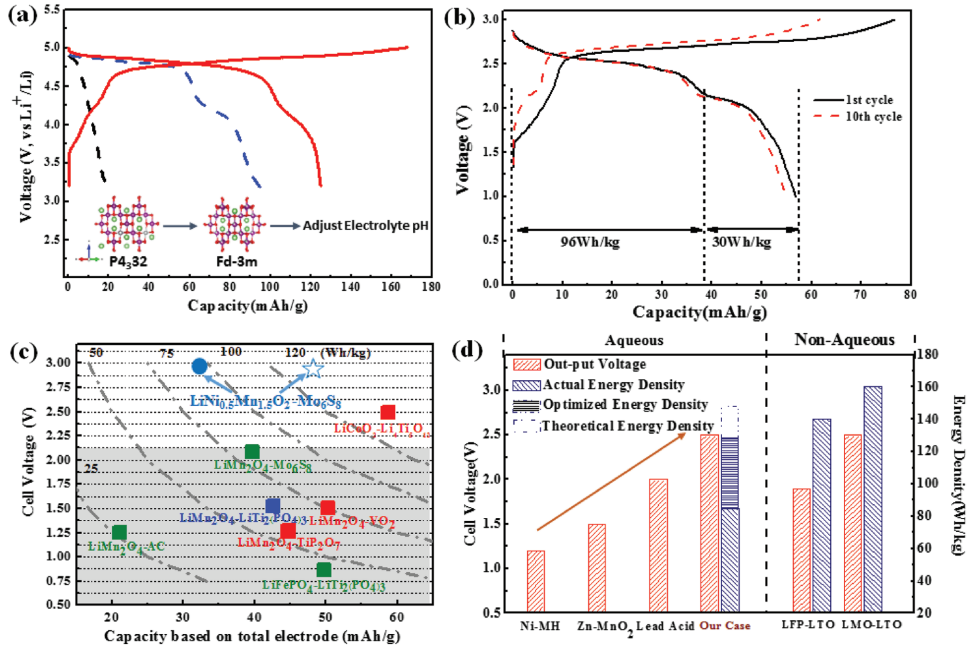

Figure 4. a) The typical voltage profile of Fd-3m $LiNi_{0.5}Mn_{1.5}O_4$ in pH-adjusted water-in-salt electrolytes at a constant current of 0.5 C with $LiTi_2(PO_4)_3$ as anode and the Ag/AgCl as the reference electrode. b) The typical voltage profile of the full aqueous Li-ion cell employing Mo_6S_8 and $LiNi_{0.5}Mn_{1.5}O_4$ as anode and cathode in pH-adjusted water-in-salt electrolytes at a constant current of 0.5 C. c) Performances comparison for ALIBs based on various electrochemical couples. d) Comparative histograms of some conventional aqueous batteries, nonaqueous lithium ion battery, and our full cell (based on electrode materials).

In summary, an intrinsic safe (Figure S7, Supporting Information) aqueous $LiNi_{0.5}Mn_{1.5}O_4/Mo_6S_8$ full cell with energy density of 126 W h kg^{-1} was demonstrated. The high voltage and energy density of $LiNi_{0.5}Mn_{1.5}O_4/Mo_6S_8$ cell is due to the large window of water-in-salt electrolyte and high potential of Fd-3m $LiNi_{0.5}Mn_{1.5}O_4$ cathodes. This safe $LiNi_{0.5}Mn_{1.5}O_4/Mo_6S_8$ cell can potentially replace some commercial flammable nonaqueous Li-ion batteries for large-scale renewable energy storage.

Experimental Section

Materials: Lithium *bis*(trifluoromethane sulfonyl) imide ($LiN(SO_2CF_3)_2$, LiTFSI) (>98%) and water (HPLC grade) were purchased from Tokyo Chemical Industry and Sigma-Aldrich, respectively. The water-in-salt aqueous electrolyte is prepared by dissolving LiTFSI in water according to molality (21 mol salt in 1 kg water, coded by abbreviated concentrations 21m). The pH value adjustment was conducted by adding 0.1% (in volume) 1 M HTFSI solution to the electrolyte.

Chevrel phase Mo_6S_8 was prepared by leaching Cu from copper Chevrel powder $Cu_2Mo_6S_8$ synthesized by solid-state synthesis method. First, $Cu_2Mo_6S_8$ precursors, CuS (99% Sigma-Aldrich), Mo (99.99% Sigma-Aldrich), and MoS_2 (99% Sigma-Aldrich) were grounded by ball-milling for 0.5 h, then the powdery mixture was pelleted under 106 Pa and sealed in Swagelok stainless steel tube, which was gradually heated to 900 °C for 24 h at 2 °C min^{-1} in argon. The products were stirred in a 6 M HCl solution for 12 h to extract Cu. Finally, the obtained powder (Chevrel Mo_6S_8) was washed with deionized water multiple times followed by drying at 100 °C overnight under vacuum. The pristine $LiNi_{0.5}Mn_{1.5}O_4$ materials were received from SAFT Corporation. The $P4_332$ structure was obtained by additional annealing of the pristine $LiNi_{0.5}Mn_{1.5}O_4$ at 700 °C for 3 d. The Fd-3m structure was obtained by fast cooling (10 °C min^{-1}) of the $LiNi_{0.5}Mn_{1.5}O_4$ calcined at 900 °C for 3 h.

Materials Characterizations: The morphology of the sample was investigated by SEM (Hitachi SU-70). XRD patterns were obtained on Bruker Smart 1000 (Bruker AXS, Inc.) using Cu Kα radiation with an airtight holder from Bruker. All the samples for ex situ XRD patterns were recovered from full aqueous Li-ion battery in 2032 coin cell configuration after electrochemical cycling. The samples were washed by Dimethoxyethane (DME) three times and then dried under vacuum for two hours. Raman measurements were performed on a Horiba Jobin Yvon Labram Aramis using a 532 nm diode-pumped solid-state laser, attenuated to give 900 mW power at the sample surface.

Electrochemical Measurements: The $LiNi_{0.5}Mn_{1.5}O_4$ and Mo_6S_8 electrodes were fabricated by compressing active materials, carbon black, and polytetrafluoroethylene at weight ratio of 8:1:1 onto the titanium mesh and the stainless steel grid, respectively. The three-electrode devices for cathode consists of $LiNi_{0.5}Mn_{1.5}O_4$ composite (about 2 mg) as working, carbon black (about 20 mg) as the counter and Ag/AgCl as the reference electrode. The anode three-electrode devices consists of Mo_6S_8 composite (about 1.5 mg) as working, 2 mm platinum disc as counter and Ag/AgCl as reference electrode. CV was carried out using CHI 600E electrochemical work station at scanning rate of 0.1 mV s^{-1} for these composite working electrodes. CV was also applied to determinate the electrochemical stability window at 10 mV s^{-1} using 316 stainless steel grid (200-mesh sieve) as both working and counter electrodes, which were thoroughly cleaned ultrasonically in high purity alcohol, and then washed three times with high purity water and dried before measurement. The potentials versus Ag/AgCl were converted to those versus standard Li^+/Li, supposing that the potential of Ag/AgCl electrode was 3.239 V versus Li+/Li.

The full ALIB cell was assembled in CR2032-type coin cell using $LiNi_{0.5}Mn_{1.5}O_4$ cathode (about 20 mg cm^{-2}), Mo_6S_8 anode (about 8 mg cm^{-2}) and glass fiber as separator. To minimize side reactions between the electrolyte and the steel coin cell components, titanium foil was put between the cathode electrode and the cell case. The charge–discharge experiments were performed on a Land BT2000 battery test system (Wuhan, China) at room-temperature.

Supporting Information

Supporting Information is available from the Wiley Online Library or from the author.

Acknowledgements

The authors gratefully acknowledge funding support from DOE ARPA-E (Grant No. DEAR0000389). The authors also acknowledge the support of the Maryland Nano Center and its NispLab. The NispLab was supported in part by the NSF as a MRSEC Shared Experimental Facility.

Received: May 2, 2016
Revised: September 21, 2016
Published online: December 14, 2016

[1] J. B. Goodenough, Y. Kim, *Chem. Mater.* **2010**, *22*, 587.
[2] M. Armand, J. M. Tarascon, *Nature* **2008**, *451*, 652.
[3] K. Xu, *Chem. Rev.* **2014**, *114*, 11503.
[4] H. Kim, J. Hong, K.-Y. Park, H. Kim, S.-W. Kim, K. Kang, *Chem. Rev.* **2014**, *114*, 11788.
[5] W. Li, J. R. Dahn, D. S. Wainwright, *Science* **1994**, *264*, 1115.
[6] W. Tang, Y. Zhu, Y. Hou, L. Liu, Y. Wu, K. P. Loh, H. Zhang, K. Zhu, *Energy Environ. Sci.* **2013**, *6*, 2093.
[7] Y. Wang, J. Yi, Y. Xia, *Adv. Energy Mater.* **2012**, *2*, 830.
[8] M. Pasta, C. D. Wessells, R. A. Huggins, Y. Cui, *Nat. Commun.* **2012**, *3*, 1149.
[9] F. Beck, P. Ruetschi, *Electrochim. Acta* **2000**, *45*, 2467.
[10] J.-Y. Luo, W.-J. Cui, P. He, Y.-Y. Xia, *Nat. Chem.* **2010**, *2*, 760.
[11] L. Suo, O. Borodin, T. Gao, M. Olguin, J. Ho, X. Fan, C. Luo, C. Wang, K. Xu, *Science* **2015**, *350*, 938.
[12] H. G. Jung, M. W. Jang, J. Hassoun, Y. K. Sun, B. Scrosati, *Nat. Commun.* **2011**, *2*, 516.
[13] S. H. Park, S. W. Oh, S. H. Kang, I. Belharouak, K. Amine, Y. K. Sun, *Electrochim. Acta* **2007**, *52*, 7226.
[14] Y. Yamada, K. Usui, K. Sodeyama, S. Ko, Y. Tateyama, A. Yamada, *Nat. Energy* **2016**, *1*, 1600129.
[15] A. Manthiram, K. Chemelewski, E.-S. Lee, *Energy Environ. Sci.* **2014**, *7*, 1339.
[16] J. Xiao, X. Chen, P. V. Sushko, M. L. Sushko, L. Kovarik, J. Feng, Z. Deng, J. Zheng, G. L. Graff, Z. Nie, D. Choi, J. Liu, J. G. Zhang, M. S. Whittingham, *Adv. Mater.* **2012**, *24*, 2109.
[17] J. Yang, X. Han, X. Zhang, F. Cheng, J. Chen, *Nano Res.* **2013**, *6*, 679.
[18] J. H. Kim, S. T. Myung, C. S. Yoon, S. G. Kang, Y. K. Sun, *Chem. Mater.* **2004**, *16*, 906.
[19] J. Song, D. W. Shin, Y. Lu, C. D. Amos, A. Manthiram, J. B. Goodenough, *Chem. Mater.* **2012**, *24*, 3101.
[20] S. K. Jeong, M. Inaba, Y. Iriyama, T. Abe, Z. Ogumi, *Electrochem. Solid State Lett.* **2003**, *6*, A13.
[21] Y. Yamada, K. Furukawa, K. Sodeyama, K. Kikuchi, M. Yaegashi, Y. Tateyama, A. Yamada, *J. Am. Chem. Soc.* **2014**, *136*, 5039.
[22] S. F. Lux, L. Terborg, O. Hachmoeller, T. Placke, H. W. Meyer, S. Passerini, M. Winter, S. Nowak, *J. Electrochem. Soc.* **2013**, *160*, A1694.

[23] D. W. McOwen, D. M. Seo, O. Borodin, J. Vatamanu, P. D. Boyle, W. A. Henderson, *Energy Environ. Sci.* **2014**, *7*, 416.
[24] L. Suo, Y.-S. Hu, H. Li, M. Armand, L. Chen, *Nat. Commun.* **2013**, *4*, 1481.
[25] S. Liu, S. H. Ye, C. Z. Li, G. L. Pan, X. P. Gao, *J. Electrochem. Soc.* **2011**, *158*, A1490.
[26] C. D. Wessells, S. V. Peddada, R. A. Huggins, Y. Cui, *Nano Lett.* **2011**, *11*, 5421.
[27] W. Li, W. R. McKinnon, J. R. Dahn, *J. Electrochem. Soc.* **1994**, *141*, 2310.
[28] H. Qin, Z. P. Song, H. Zhan, Y. H. Zhou, *J. Power Sources* **2014**, *249*, 367.
[29] L. Chen, Q. Gu, X. Zhou, S. Lee, Y. Xia, Z. Liu, *Sci. Rep.* **2013**, *3*, 1946.
[30] H. Wang, K. Huang, Y. Zeng, S. Yang, L. Chen, *Electrochim. Acta* **2007**, *52*, 3280.
[31] Y. G. Wang, Y. Y. Xia, *J. Electrochem. Soc.* **2006**, *153*, A450.
[32] B. Guiose, F. Cuevas, B. Decamps, E. Leroy, A. Percheron-Guegan, *Electrochim. Acta* **2009**, *54*, 2781.
[33] R. M. Dell, *Solid State Ionics* **2000**, *134*, 139.